Journal of Catalysis **209,** 289–305 (2002)
doi:10.1006/jcat.2002.3585

Reaction Paths in the Hydrogenolysis of Acetic Acid to Ethanol over Pd(111), Re(0001), and PdRe Alloys

Venkataraman Pallassana and Matthew Neurock[1]

Department of Chemical Engineering, University of Virginia, Charlottesville, Virginia 22903

Received August 3, 2001; revised February 22, 2002; accepted March 1, 2002

Nonlocal density functional theory (DFT) calculations are used to examine alternative mechanisms for the hydrogenolysis of acetic acid to ethanol over Pd. The overall surface reaction energies, at low surface coverage, are computed for a number of different possible paths by which acetic acid may be converted to ethanol over Pd(111). Binding energies of the various oxygenated C_2 intermediates formed along these paths are also reported. The overall reaction energies were used to propose a plausible mechanism for acetic acid hydrogenolysis. In the postulated mechanism, acetic acid dissociates to form an acetyl surface intermediate. The acetyl intermediate is then subsequently hydrogenated to ethanol via the formation of an acetaldehyde surface intermediate. Detailed reaction coordinate calculations were used to isolate the transition states and calculate activation barriers for acetic acid dissociation to acetyl ($\Delta E^{act} = +142$ kJ/mol) and acetyl hydrogenation to acetaldehyde ($\Delta E^{act} = +66$ kJ/mol) over Pd(111). Experimental observations and DFT calculations suggest that these two steps are likely to be rate determining in acetic acid hydrogenolysis. The barriers and overall reaction energies for these same steps are also computed on Re(0001) and pseudomorphic overlayers of Pd on Re (Pd_{ML}/Re(0001)) as well. The results suggest that the C–OH bond-dissociation reaction is more favored over Re(0001) since it has a more open d band. However, bond-association reactions such as acetyl hydrogenation are more favored over Pd_{ML}/Re(0001), which has an electronic d-band structure similar to that of a noble metal. The optimal balance may require a Pd/Re alloy. Calculations performed over a $Pd_{0.66}Re_{0.33}$ alloy demonstrate a nominal barrier for both C–OH bond breaking and C–H bond formation. This may be ideal for acetic acid hydrogenolysis to ethanol. Rhenium ensembles, however, should be avoided as they lead to acetic acid decarboxylation.

1. INTRODUCTION

Alkanediols such as ethylene glycol, 1,3-propanediol, and 1,4-butanediol are important precursors to the synthesis of polyesters and polyurethanes. An economically attractive route to the synthesis of higher alcohols, such as 1,4-butanediol, is through the hydrogenation of carboxylic acids. For example, in the Kvaener John Brown and the Davy–McKee processes, it has been shown that 1,4-butanediol can be produced via the hydrogenation of maleic acid (or its esters) (18, 44, 48). 1,4-Butanediol is subsequently used to synthesize tetrahydrofuran, an important intermediate in the manufacture of spandex fibers such as Lycra (9, 55, 56). In 1997, 740,000 metric tons of 1,4-butanediol (1,4-BDO) was produced worldwide, and the demand for 1,4-BDO has been slated to increase steadily at the rate of 5–7% a year (55). There is a very strong economic incentive in understanding the catalytic process involved in the synthesis of 1,4-BDO from its acidic precursors.

Numerous catalytic systems have been proposed as efficient catalysts for the hydrogenolysis of caboxylic acids (or esters) to alcohols. Cu-chromite based catalysts have been typically used for the vapor-phase hydrogenolysis of acids (30, 31). Since the disposal of spent chromite-based catalysts presents a considerable environmental cost, there is a growing tendency to replace these catalysts with more benign catalytic materials. In the 1980s and 1990s, DuPont showed that transition-metal-based bimetallic catalysts, such as Pd–Re or Ru–Re particles, can be used as catalysts for the hydrogenation of maleic acid to tetrahydrofuran (26, 27, 47). Subsequently, Kitson and Williams also demonstrated that Pd–Re-based catalysts are not only active for maleic acid hydrogenolysis but show good activity and selectivity in the hydrogenolysis of other carboxylic acids, such as acetic acid, propionic acid, butyric acid, and heptanoic acid to their analogous alcohols (22). This suggests that the governing mechanisms that control activity and selectivity for carboxyl group hydrogenolysis may be analogous for a homologous set of carboxylic acids. More recently, Vannice and co-workers have shown that Pt particles dispersed on TiO_2 may also be used for the selective hydrogenolysis of acetic acid to ethanol (43).

The intrinsic catalytic activity for the hydrogenolysis of higher molecular weight carboxylic acids is likely to be similar for series of related organic acids. Acetic acid may serve as a model system to understand the catalytic reactions for many other carboxylic acids. Over the past few decades, the adsorption and reactions of acetic acid (and related esters) have been studied extensively on both single crystal (1, 8, 14, 19–21, 46, 51) and supported transition metal systems

[1] To whom correspondence should be addressed. Fax: (804) 982-2658. E-mail: mn4n@virginia.edu.

0021-9517/02 $35.00

(2, 10, 15, 24, 32, 43, 53). These studies have provided significant insights into the mechanism for decomposition of carboxylic acids and aldehydes (11, 12, 14, 50). They have also allowed identification of possible intermediates formed during carboxylic acid hydrogenation over monometallic transition metal systems (2, 10, 15, 32, 43). There are a few experimental studies which examine the detailed pathways for carboxylic acid (and ester) hydrogenolysis over supported monometallic catalysts (2, 3, 15, 32, 43, 57). However, to our knowledge, there is no published work that examines the mechanism for hydrogenolysis of acids over bimetallic systems. Understanding the synergy between the individual metals such as Pd and Re, and their role in influencing the overall activity and selectivity for carboxylic acid hydrogenolysis, may provide insights into tailoring newer catalytic systems with improved properties.

First-principles density functional theory (DFT) is emerging as a powerful tool for probing reaction mechanisms on metal surfaces. In this paper, we use DFT to explore alternative paths for the hydrogenolysis of acetic acid to ethanol over well-defined Pd(111) surfaces. We examine a rather comprehensive set of reaction paths to discern which steps are feasible. We then postulate what appears to be an energetically favorable catalytic cycle for acetic acid hydrogenolysis over Pd(111). Detailed reaction coordinate calculations are used to isolate key transition states within the catalytic cycle. We subsequently examine how alloying the surface with a second metal, such as rhenium, influences the activity and selectivity for hydrogenolysis. We discuss only the reaction energetics in this paper. Subsequent studies will use the results outlined here in a kinetic Monte Carlo simulation to track the surface coverage as a function of time as well as the reaction rates for this system.

2. COMPUTATIONAL DETAILS

All results discussed in the paper were determined using gradient-corrected DFT quantum-chemical calculations. Chemisorption and reactivity on well-defined metal surfaces were modeled using clusters as well as periodic slabs. The exchange-correlation potential used in the local density approximation is that from Vosko *et al.* (54). Nonlocal gradient corrections to the exchange-correlation energy were calculated self-consistently using the Becke and Perdew functionals (6, 7, 41) (for cluster calculations) and the Perdew–Wang (PW91) model (42) (for periodic slab calculations). The atomic orbital basis sets, used in the cluster calculations, were contracted polarized gaussian-type functions of double-zeta quality. These basis sets were optimized specifically for DFT calculations and tend to perform at levels higher in accuracy than traditional basis sets (4, 5). They are also optimized to minimize basis-set superposition error (4, 5). Scalar relativistic corrections were incorporated through the use of frozen-core pseudopotentials for all core electrons of the transition metal elements.

For 2-D periodic systems, such as metal surfaces, the valence orbital states are best approximated by Bloch functions (23). Plane-wave basis sets are, therefore, more expedient in describing the valence electronic states for these systems (40). A 40-Rydberg cutoff energy was found to be adequate in the plane-wave basis expansion and was used in all the periodic-slab calculations reported herein. The core states of the metal are not critical in describing adsorbate–surface bonding and are therefore described by a frozen-core, norm-conserving pseudopotential in the periodic slab calculations (25, 40). For a (1×1) unit cell, the total energy of the system was found to be convergent for 54 k-points in the first Brillouin zone.

All self-consistent field calculations (SCF) in the cluster approach were converged to 0.02 kJ/mol, and the geometry was optimized to a gradient less than 13 kJ/Å. For the periodic slab calculations, the SCF was converged to 1×10^{-3} kJ/mol and the geometry to 28 kJ/Å. For the cluster calculations, the geometries were determined by constraining the metal surface to the bulk metal–metal bond distances and completely optimizing the adsorbate. The 18- and 19-metal-atom cluster models used in this paper are composed of two constrained metal layers. The periodic slab model has a three-metal layer. In both the cluster and slab models, the metal atoms to which the adsorbate is directly bound have their complete set of nearest neighbors. For the three-metal-layer slab model, the top two metal layers were optimized completely, while the third metal layer was constrained to the bulk interatomic distances. A comparison of the binding energies computed using the cluster and periodic slab models is provided in Table 1. The differences are within the limits of accuracy of the DFT methodology (33, 58). The 18- and 19-metal-atom cluster models used herein appear to provide reasonable estimates of the adsorption energies.

All of the bare cluster calculations were performed spin-unrestricted. The most favorable spin multiplicity of the cluster was determined by performing a series of calculations with different spin states to find the lowest energy state. For a number of the cluster–adsorbate calculations, including hydrogen, acetate, and acetic acid, we found that the spin multiplicity was the same as that of the bare cluster. The bare cluster spin multiplicity was, therefore, used for the cluster–adsorbate systems. The resulting spin electronic occupations for the converged systems were found to be consistent. Since the metals examined in this paper are nonmagnetic in the bulk, all the periodic slab calculations were performed spin-unpolarized.

Details on the implementation of DFT in the DGauss program, used for the cluster calculations, may be found in Refs. (4, 5). Periodic slab calculations were performed using the plane-wave pseudopotential program VASP developed at the Technical University of Vienna (25).

TABLE 1

DFT-Computed Binding Energies (B.E.) of Intermediates That May Form during the Hydrogenolysis of Acetate on Pd(111)

Species	Structure[a] reference	Adsorption mode and site	B.E.[b] of cluster (kJ/mol)	B.E.[c] of slab (kJ/mol)
Acetate	A	di-σ (O,O) bridge	−212	−220
Acetic acid	B	di-σ (O,O) bridge	−25	−20
Acetoxy intermediate of ethane-1,1-diol	C	η^1(C) atop	−145	—
Dioxyethylidene	D	di-σ (O,O) bridge	−264	—
Alkoxy intermediate of 1,1-ethane-diol	E	η^3(O) 3-fold fcc	−159	—
Acetyl	F, G	$\eta^2\eta^1$(C,O) 3-fold fcc	−176	−194
Acetaldehyde	H, I, J	di-σ (C,O)	−29	−25
Hydroxyethylidyne	K	η^2(C) bridge	−318	—
Ethoxy	L	η^3(O) 3-fold fcc	−151	−166
Acetoxy	M	η^1(C) atop	−135	−133
Ethanol	N	η^1(O) atop	−21	−17
Hydroxyl	F, I	η^3(O) 3-fold fcc	−251	—
Water	G, J, K, L, M, N	η^1(O) atop	−31	−30
Oxygen atom	H	η^3 3-fold fcc	−375	—
Hydrogen atom		η^3 3-fold fcc	−257	−267

[a] Structure names are with reference to Figs. 1–3.

[b] Binding energies computed using fixed two-layer Pd(12, 7) and Pd(12, 6) cluster models of the Pd(111) surface.

[c] Binding energies computed using periodic density functional theory calculations. Coverage = 0.25 monolayer, corresponding to a (2 × 2) unit cell.

The binding energies of the intermediates were computed for adsorption modes that are expected to be the most favorable adsorption configuration on Pd(111). Binding energies were computed using the expression

$$\Delta E_{\text{binding energy}} = E_{\text{cluster (or slab)}+\text{adsorbate}} - E_{\text{cluster (or slab)}} - E_{\text{adsorbate}}, \quad [1]$$

where $\Delta E_{\text{binding energy}}$ is the binding energy of the adsorbate, $E_{\text{cluster (or slab)}+\text{adsorbate}}$ is the total energy of the adsorbate bound to the Pd cluster or slab, $E_{\text{cluster(or slab)}}$ is the total energy for the bare Pd cluster or Pd slab, and $E_{\text{adsorbate}}$ is the total energy of the adsorbate in the vapor phase. All calculations were performed using spin polarization and the most favorable spin multiplicity of the system was explicitly determined.

The calculated binding energies were used along with gas-phase reaction energies to calculate the surface reaction energies for all of the elementary steps shown in Fig. 1. The surface reaction energies on Pd(111) were calculated from the expression

$$\Delta E_{\text{rxn}}^{\text{surface}} = \Delta E_{\text{rxn}}^{\text{vapor phase}} + \sum \Delta E_{\text{binding energy}}^{\text{products}} - \sum \Delta E_{\text{binding energy}}^{\text{reactants}}, \quad [2]$$

where ΔE_{rxn} denotes the overall reaction energy for the elementary step, the superscript "surface" denotes the reaction energy estimated on the Pd(111) surface (using Eq. [2]), and the superscript "vapor phase" denotes the reaction energy calculated using DFT in the absence of the metal surface; $\Delta E_{\text{binding energy}}$ corresponds to the binding energy of the adsorbed intermediate on the Pd(111) cluster or slab.

It is important to note that calculating the surface reaction energies using Eq. [2] neglects the effect of lateral interactions between surface species. The computed value approximates the overall surface reaction energy for an elementary step in the low surface coverage limit. In this limit all the reactant and product species are isolated on the metal surface. For bimolecular or higher molecularity elementary reactions of surface-bound species, the reacting entities are generally in close proximity on the surface. For such cases, the lateral interaction energy between the species can be important. Lateral interactions between surface-bound species typically range from 15 to 40 kJ/mol. As an approximation, we have neglected lateral interaction energies in computing the surface reaction energies for the elementary steps in Fig. 1.

Transition state structures for individual elementary steps were isolated using the nudged-elastic-band technique as implemented in VASP. This approach involves discretizing the path between the reactant and product states into a sequence of structural images. The initial starting structure for each image is determined based on its distance along the linear path between reactant and product state. The transition state search involves optimizing each image along the direction perpendicular to the vector that connects two neighboring images. All of the forces, except those along the hypertangent, are optimized to zero.

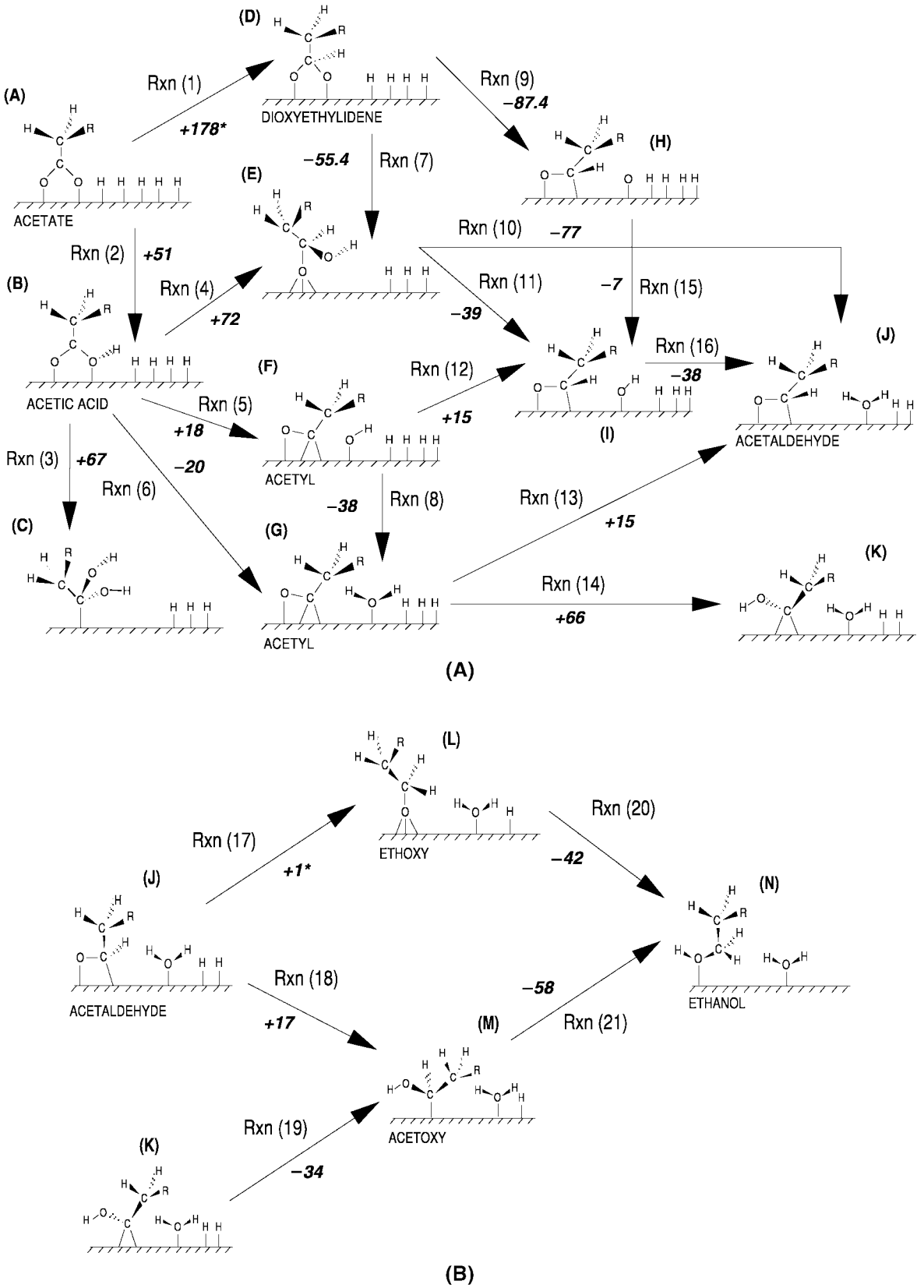

FIG. 1. (A) Alternative reaction paths for the hydrogenolysis of acetate (R=H) to ethanol over Pd(111). (B) Continuation of alternative reaction paths for the hydrogenolysis of acetate (R=H) to ethanol over Pd(111). All energies are in kJ/mol.

3. RESULTS AND DISCUSSION

3.1. Analysis of Divergent Paths for the Hydrogenolysis of Acetic Acid to Ethanol over Pd(111)

As a first step toward determining the energetically *most favorable* path for carboxylic acid hydrogenolysis, we mapped out various different elementary paths by which acetic acid may be converted to ethanol over a Pd(111) surface. Figure 1 schematically illustrates the network of steps by which acetic acid can be hydrogenated to ethanol on Pd(111). It includes both C–O bond breaking and hydrogenation steps. For example, the scission of the C–O bond of acetic acid may occur directly, or it may be initiated by the addition of surface hydrogen. Many of the surface intermediates that form in the path to ethanol undergo hydrogenation. The initial attack of surface hydrogen can occur at different adsorbate centers, resulting in different surface intermediates. These divergent paths set up various alternative mechanisms for the overall hyrogenolysis of acetic acid, as is illustrated in Fig. 1.

We recognize that the most rigorous theoretical way to elucidate the operative mechanism for hydrogenolysis is to calculate the activation barriers for all of the possible elementary steps in Fig. 1 to determine the kinetics. This would require the isolation of transition states for over 20 individual elementary reaction steps. The calculation of so many transition states is beyond our present computational resources. In this paper, we therefore use the overall surface reaction energies, i.e., the ΔE_{rxn}, on Pd(111) as a guide to elucidate the *most plausible* steps in the mechanism for acetic acid hydrogenolysis over Pd(111). Transition state search calculations are then performed for steps that appear limiting along this most plausible reaction path.

DFT-cluster calculations were used to compute the binding energies of various different surface intermediates that can form during acetic acid hydrogenolysis to ethanol. The various intermediates are identified in Fig. 1. Note that the surface reaction pathways shown in Fig. 1 only depict the direct channels that lead to ethanol. Other side reactions that lead to C_1 products such as CO and CO_2 are not shown in this figure. These reactions, however, are important in determining the overall selectivity during hydrogenolysis and are briefly discussed in Section 3.5.

First-principles DFT calculations were performed using the Pd(12, 6) or Pd(12, 7) clusters models of the Pd(111) surface (see Figs. 2 and 3). In previous papers, we have

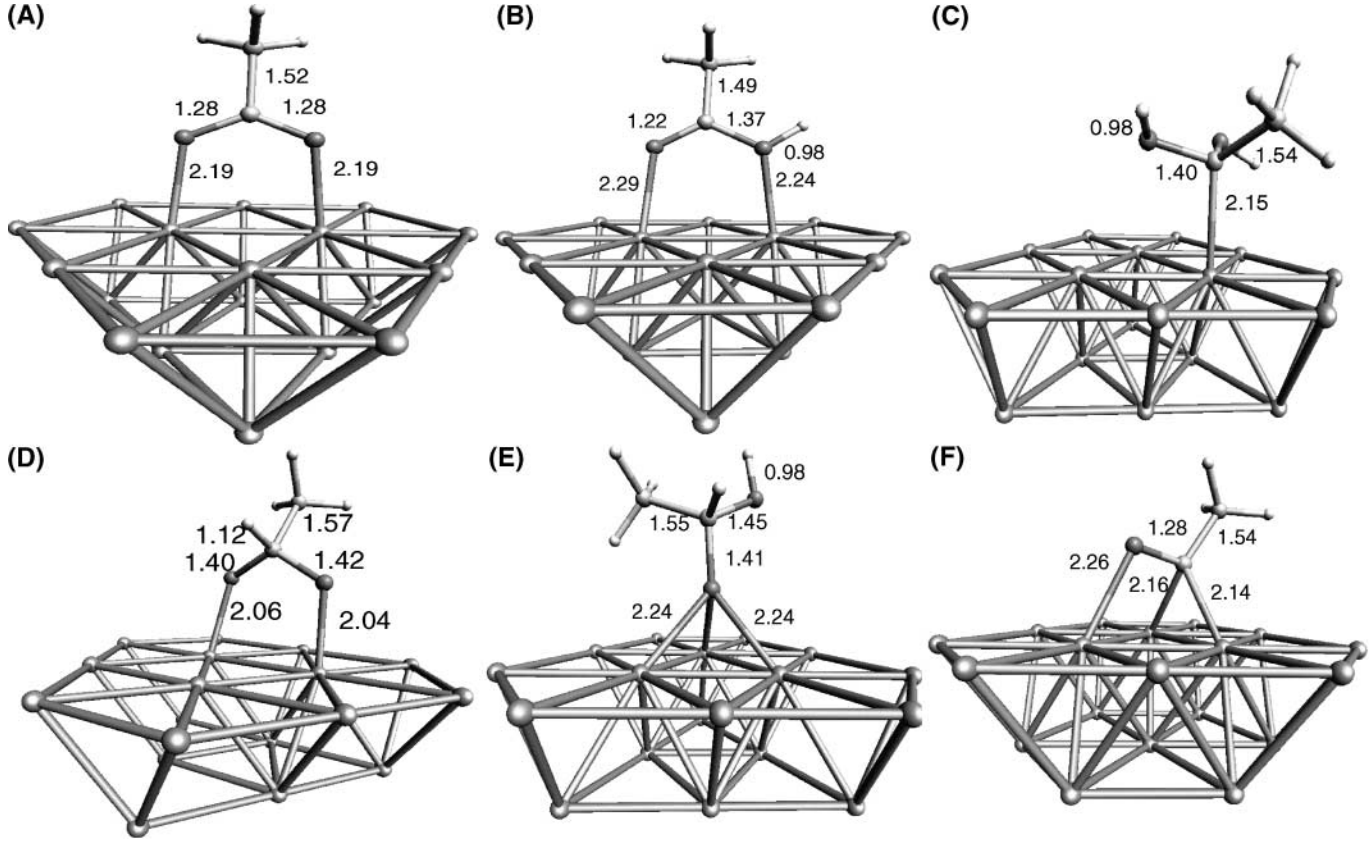

FIG. 2. DFT-optimized geometry of possible surface intermediates that may be formed during the hydrogenolysis of acetate over Pd(111): (A) acetate, (B) acetic acid, (C) acetoxy intermediate of 1,1-ethanediol, (D) dioxyethylidene, (E) alkoxy intermediate of 1,1-ethanediol, and (F) acetyl.

shown that reliable binding energies, representative of low coverage adsorption on the periodic (111) surface, are predicted well by these 19- and 18-metal-atom cluster models (33, 35, 38). Table 1 also shows a comparison of adsorption energies calculated using the 19-metal-atom cluster and full periodic slab models. The results show that the differences are within 10–20 kJ/mol. From Table 1 it appears that the differences in binding energies between the cluster and slab model are slightly higher for the more strongly bound intermediates such as acetyl and ethoxy. This is likely because we have included surface relaxation effects in the slab model, which are important for more accurate predictions of binding energies. Adsorbate-induced relaxation effects on a semiinfinite metal surface cannot be justifiably captured using the cluster model and were therefore ignored during the cluster calculations. The binding energies calculated using the cluster model, however, still appear to be reasonable and compare fairly well with those calculated by periodic slab calculations. The DFT-optimized geometry for the various intermediates are shown in Figs. 2 and 3.

Table 1 summarizes the DFT-calculated binding energies and the adsorption modes examined for the various different intermediates. From Table 1, we find that the closed-shell intermediates such as acetaldehyde, acetic acid, water, and ethanol are all relatively weakly bound to the surface either through van der Waals interactions that occur between the lone pair of electrons on the hydroxyl oxygen or through weak π-bonded interactions of the C=O group. The calculated adsorption energies range between 20 and 35 kJ/mol. Stuve *et al.* estimate that the adsorption energy of water on clean Pd(100) is about −40 kJ/mol (52). Our calculated adsorption energy of −31 kJ/mol on the more close-packed Pd(111) surface therefore appears to be a reasonable estimate of the binding energy. The adsorption energy of acetaldehyde and ethanol estimated from TPD experiments on Pd(110) are −44 kJ/mol and −38 kJ/mol, respectively (49, 50). Our computed adsorption energies of −29 kJ/mol (acetaldehyde) and −21 kJ/mol (ethanol) on Pd(111) are slightly weaker than the experimental estimates. One would expect that the adsorption energies would be somewhat higher on the (110) surface since it is the more open surface. In addition, it is also well known that DFT tends to underpredict weaker van der Waals interactions. The unsaturated intermediates are very strongly bound to the Pd(111), having binding energies ranging between 100 and 450 kJ/mol. Among the species examined here, atomic oxygen is the most strongly bound surface intermediate on Pd(111) with a computed binding energy of −375 kJ/mol. Binding energies of the other unsaturated intermediates are tabulated in Table 1.

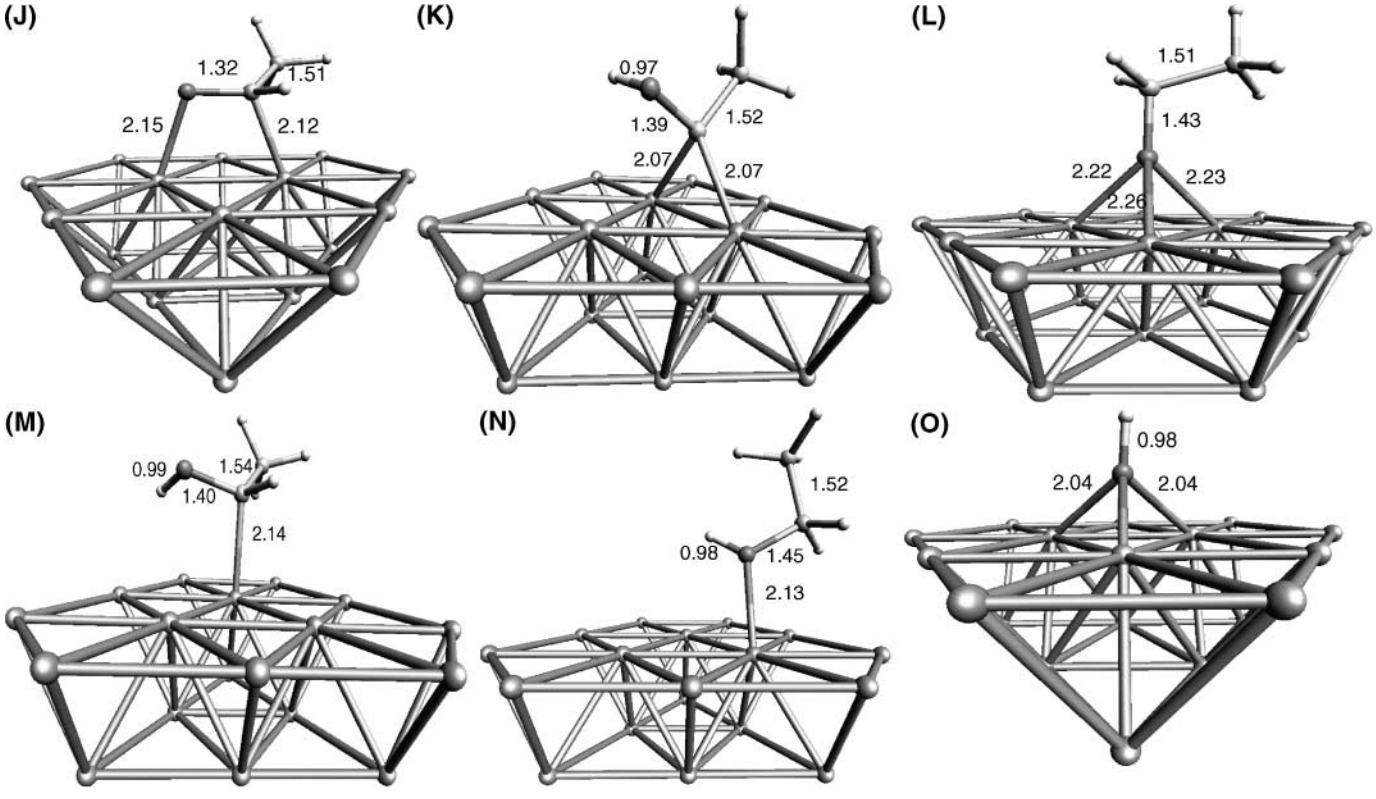

FIG. 3. DFT-optimized geometry of possible surface intermediates that may be formed during the hydrogenolysis of acetate over Pd(111): (J) acetaldehyde, (K) hydroxyethylidyne, (L) ethoxy, (M) acetoxy, (N) ethanol, and (O) hydroxyl.

TABLE 2

Surface Reaction Energetics for the Hydrogenolysis of Acetate on Pd(111) Computed Using DFT Cluster Calculations

Elementary reaction[a]	Description of elementary step	Surface reaction energy (kJ/mol)
Rxn (1)	acetate α C–H bond formation to dioxyethylidene $CH_3COO^* + H^* \rightarrow CH_3CHOO^* + *$	+178
Rxn (2)	acetate O–H bond formation to acetic acid $CH_3COO^* + H^* \rightarrow CH_3COOH^* + *$	+51
Rxn (3)	acetic acid O–H bond formation to the acetoxy intermediate of ethane-1,1-diol $CH_3COOH^* + H^* \rightarrow CH_3C(OH)_2^* + *$	+67
Rxn (4)	acetic acid α C–H bond formation to the alkoxy intermediate of ethane-1,1-diol $CH_3COOH^* + H^* \rightarrow CH_3CH(OH)O^* + *$	+72
Rxn (5)	acetic acid α C–OH bond breaking to form acetyl + OH $CH_3COOH^* + * \rightarrow CH_3CO^* + OH^*$	+18
Rxn (6)	hydrogen-assisted acetic acid αC–OH bond breaking to form acetyl + H_2O $CH_3COOH^* + H^* \rightarrow CH_3CO^* + H_2O^*$	−20
Rxn (7)	dioxyethylidene O–H bond formation $CH_3CHOO^* + H^* \rightarrow CH_3CH(OH)O^* + *$	−55.4
Rxn (8)	$OH^* + H^* \rightarrow H_2O^* + *$	−38
Rxn (9)	dioxyethylidene α C–O bond breaking to form acetaldehyde and surface oxygen $CH_3CHOO^* + * \rightarrow CH_3CHO^* + O^*$	−87.4
Rxn (10)	hydrogen-assisted C–OH bond breaking of alkoxy intermediate of 1,1-ethanediol to form acetaldehyde and water $CH_3CH(OH)O^* + H^* \rightarrow CH_3CHO^* + H_2O^*$	−77
Rxn (11)	C–OH bond breaking of alkoxy intermediate of 1,1-ethanediol to form acetaldehyde and surface hydroxyl $CH_3CH(OH)O^* + * \rightarrow CH_3CHO^* + OH^*$	−39
Rxn (12)	acetyl α C–H bond formation to acetaldehyde $CH_3CO^* + H^* \rightarrow CH_3CHO^* + *$	+15
Rxn (13)	acetyl α C–H bond formation to acetaldehyde $CH_3CO^* + H^* \rightarrow CH_3CHO^* + *$	+15
Rxn (14)	acetyl O–H bond formation to hydroxy-ethylidyne $CH_3CO^* + H^* \rightarrow CH_3C(OH)^* + *$	+66
Rxn (15)	$O^* + H^* \rightarrow OH^* + *$	−7
Rxn (16)	$OH^* + H^* \rightarrow H_2O^* + *$	−38
Rxn (17)	acetaldehyde C–H bond formation to ethoxy $CH_3CHO^* + H^* \rightarrow CH_3CH_2O^* + *$	+1
Rxn (18)	acetaldehyde O–H bond formation to acetoxy $CH_3CHO^* + H^* \rightarrow CH_3CH(OH)^* + *$	+17
Rxn (19)	hydroxy-ethylidyne C–H bond formation to acetoxy $CH_3C(OH)^* + H^* \rightarrow CH_3CH(OH)^* + *$	−34
Rxn (20)	ethoxy O–H bond formation to ethanol $CH_3CH_2O^* + H^* \rightarrow CH_3CH_2OH^* + *$	−42
Rxn (21)	acetoxy C–H bond formation to ethanol $CH_3CH(OH)^* + H^* \rightarrow CH_3CH_2OH^* + *$	−58

[a] Reaction number assignments are with reference to Fig. 1.

Table 2 summarizes the energies of reaction for each of the elementary surface reaction steps that are schematically illustrated in Fig. 1. The surface reaction energies were computed using Eq. [2]. It is known experimentally that acetic acid readily dissociates to form acetate on the bare Pd(111) surface, even at subambient temperatures (14). We have therefore used acetate as a starting point in analyzing the divergent paths for carboxyl group hydrogenolysis.

3.1.1. Reaction paths for acetate on Pd(111). In the presence of hydrogen, surface-bound acetate can undergo a number of different possible reactions. These include:

(a) direct C–O bond breaking to form surface-bound acetyl and atomic oxygen;

(b) hydrogen-assisted C–O bond breaking to form surface-bound acetyl and hydroxyl species;

(c) hydrogen addition to the α-carbon of acetate to form dioxyethylidene [Rxn (1) in Fig. 1A];
(d) hydrogen addition to carboxyl oxygen to form acetic acid [Rxn (2) in Fig. 1A]; and
(e) β C–H bond breaking of acetate.

DFT calculations indicate that the direct C–O bond breaking of acetate to form acetyl and atomic oxygen is endothermic (~76 kJ/mol). This pathway is not illustrated in Fig. 1A. If the dissociation of acetate is mediated by surface hydrogen, to form acetyl and hydroxyl, the surface reaction energy is slightly less endothermic (+69 kJ/mol). Table 2 suggests that the hydrogenation of acetate to dioxyethylidene [Rxn (1)] is the least favorable reaction step with an endothermicity of +178 kJ/mol on Pd(111). This reaction is considerably more endothermic than the hydrogenation of acetate back to acetic acid [Rxn (2)], which was found to be endothermic by 51 kJ/mol. Since the reaction to form dioxyethylidene is 178 kJ/mol uphill, this suggests that the minimum activation barrier for hydrogenation of acetate to dioxyethylidene [Rxn (1)] is at least 178 kJ/mol. Experimentally, the reaction-limited desorption of acetic acid by the reaction of surface-bound acetate and atomic hydrogen is known to occur at about 270 K on Pd(111) (11, 14). The activation barrier for this reaction is estimated to be roughly 67–70 kJ/mol. Based on the surface reaction energies, it appears that the hydrogenation of acetate to acetic acid is likely to be significantly more favorable than the formation of dioxyethylidene and slightly more favorable than acetate C–O bond breaking to form acetyl.

β C–H bond breaking of acetate is the precursor to an important unselective decomposition route for acetate on Pd(111) and is discussed in Section 3.5.

3.1.2. Reaction paths for acetic acid on Pd(111). Acetic acid on Pd(111) can also undergo a multitude of different surface reactions in the presence of excess surface hydrogen. These paths include:

(a) dissociation of acetic acid via C–OH bond breaking to form surface acetyl and hydroxyl species;
(b) hydrogen-mediated dissociation of acetic acid via C–OH bond breaking to form acetyl and water;
(c) C=O bond breaking of acetic acid to form hydroxyethylidyne (see structure K in Fig. 3) and surface oxygen;
(d) addition of hydrogen to the α-carbon of acetic acid to form the alkoxy intermediate of 1,1-ethane-diol (see structure E in Fig. 2); and
(e) addition of hydrogen to the C=O oxygen of acetic acid to form the acetoxy intermediate of 1,1-ethane-diol (see structure C in Fig. 2).

The C–OH bond of acetic acid may break directly to form a surface acetyl species and a surface-bound hydroxyl group, as depicted by Rxn (5) (see Fig. 1A). Calculations suggest that this reaction is mildly endothermic at +18 kJ/mol. In an analogous path, atomic hydrogen bound to the metal surface can assist in the activation of the C–OH bond activation step by reacting with the hydroxyl group that forms in a concerted manner to produce water. This is depicted as Rxn (6) in Fig. 1A. This reaction is exothermic by 20 kJ/mol. The C=O bond breaking of acetic acid to form hydroxyethylidyne (see structure K in Fig. 3) and atomic oxygen is energetically the most uphill path with a reaction endothermicity of +91 kJ/mol. This is not surprising because activating the C=O double bond would require significantly more energy than what is required to break the C–OH single bond.

As an alternative to these bond-breaking pathways, acetic acid may react with surface-bound hydrogen. There are two possible sites for the attack of atomic hydrogen. If the hydrogen atom adds to the α-carbon position [Rxn (4)], the intermediate formed is 1,1-ethanediol (see species E in Figs. 1 and 2). DFT results indicate that this elementary step is highly endothermic (+72 kJ/mol). If the hydrogen attacks the oxygen of the carbonyl group on acetic acid, the reaction is still fairly endothermic at +67 kJ/mol [Rxn (3)]. This reaction results in the formation of the acetoxy intermediate of ethane-1,1-diol. Based on the overall energetics computed here, it appears that the C–OH bond-breaking of acetic acid by the elimination of either a hydroxyl group or water is the energetically *most favorable* route on Pd(111) for acid hydrogenolysis. This mechanism results in the formation of the acetyl surface intermediate (see structure F in Fig. 2).

3.1.3. Reaction paths for acetyl on Pd(111). In the presence of surface-bound hydrogen, the acetyl surface intermediate formed by the dissociation of acetic acid can hydrogenate to produce ethanol. Again, there are two possible sites for hydrogen attack, the acetyl α-carbon or the terminal oxygen atom. The addition of hydrogen to the α-carbon atom results in the formation of acetaldehyde. DFT calculations indicate that this reaction [Rxn (12) in Fig. 1A] is mildly endothermic by 15 kJ/mol. Alternatively, the addition of hydrogen to the oxygen end of acetyl results in the formation of hydroxyethylidyne (species K in Fig. 3). This reaction step [Rxn (14)] is estimated to be significantly more endothermic with a reaction energy of +66 kJ/mol. The energetically more favorable channel therefore appears to be the hydrogenation of acetyl to acetaldehyde.

Instead of hydrogenation, acetyl can also decompose on the metal surface to form CO. UHV surface science studies by Barteau and co-workers (11, 14, 50) suggest that the formation of CO from acetaldehyde occurs via the formation of the acetyl surface intermediate. The acetyl species undergoes C–C bond scission at 490 K to form surface-bound CO and methyl species.

3.1.4. Reaction paths for acetaldehyde on Pd(111). Acetaldehyde, when formed, may be hydrogenated to ethanol, either via the ethoxy intermediate (species L in Fig. 3) or the acetoxy intermediate (species M in Fig. 3), depending

on where the first hydrogen atom inserts into acetaldehyde. Our calculations suggest that the hydrogenation of acetaldehyde to ethoxy is thermoneutral (1 kJ/mol), while the hydrogenation of acetaldehyde to acetoxy is endothermic (+17 kJ/mol). Due to this relatively small difference in the reaction energy, it is difficult to say which is likely to be the dominant pathway for the hydrogenation of acetaldehyde on Pd(111). The differences between these two paths may be more pronounced over other metals. In the final step, the acetoxy or ethoxy intermediate is hydrogenated to ethanol. The hydrogenation of ethoxy to ethanol is exothermic by 42 kJ/mol, while the hydrogenation of acetoxy to ethanol is exothermic by 58 kJ/mol.

3.1.5. A plausible catalytic cycle. By analyzing the reaction energies associated with each step in Fig. 1, we were able to prune the detailed set of reaction pathways into a set of energetically acceptable steps. All of the highly endothermic paths were ruled out in that their activation barriers would likely be prohibitive. The remaining steps form a plausible catalytic cycle for acetic acid hydrogenolysis. The resulting cycle can be broken down into two basic paths: C–O hydrogenolysis to form the aldehyde and subsequent hydrogenation of the aldehyde to ethanol. Based on our analysis of the overall reaction energies presented in Figs. 1 and 2, it appears that the most favored path on Pd(111) is via the C–OH bond breaking of acetic acid to form surface-bound acetyl and hydroxyl species [Rxn (5)]. The hydroxyl intermediate can react with a surface hydrogen atom to form water [Rxn (8)]. These two steps could also possibly occur in a single concerted step, whereby water is eliminated during acetic acid dissociation to acetyl [Rxn (6) in Fig. 1A]. The acetyl intermediate can then undergo hydrogenation to acetaldehyde. The acetaldehyde species can either desorb or undergo further hydrogenation to form ethanol. On the basis of these DFT calculations, it is difficult to identify whether the hydrogenation of acetaldehyde proceeds via the acetoxy or ethoxy intermediate. However, the formation of ethoxy appears to be slightly more favorable than the formation of acetoxy. This postulated cycle of elementary reaction steps for the hydrogenolysis of acetic acid to ethanol is shown in Fig. 4.

An important point of interest here is that all of the surface intermediates identified in the reaction path of Figure 4 have been observed spectroscopically under UHV conditions on the well-defined Pd(111) surface.

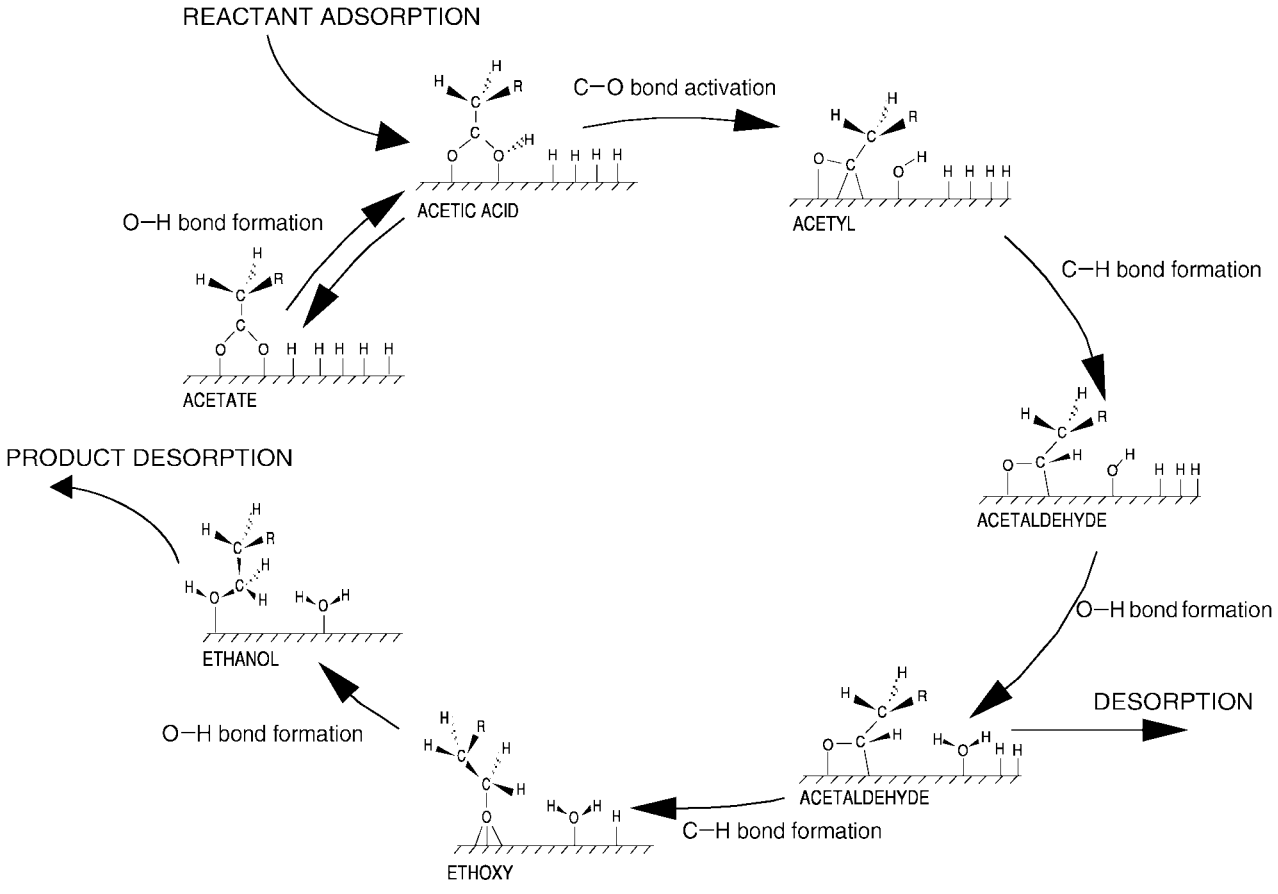

FIG. 4. Proposed elementary mechanism for the hydrogenolysis of acetic acid to ethanol over Pd(111), based on DFT-calculated overall surface reaction energies.

Acetic acid and acetate have been identified on Pd(111) while studying the decomposition of acetic acid (11, 14). Acetyl species are known to be formed by the surface reactions of both acetaldehyde and ethanol (11, 12, 13, 14). Ethoxy was formed by the dissociation of ethanol over Pd(111) (13). Although the spectroscopic identification of these intermediates does not necessarily confirm our proposed reaction mechanism, it, at the very least, supports the hypothesis that these species *can* be formed as intermediates during acetic acid hydrogenolysis on Pd(111).

3.2. Plausible Rate-Determining Steps

By analyzing the energetics for each of the steps in the proposed cycle, along with known experimental evidence, we can begin to suggest possible rate-limiting steps. The hydrogenation of acetate to acetic acid on Pd(111) occurs at about 270 K on Pd(111) under UHV conditions (11, 14). The activation barrier for this process is estimated to be less than 75 kJ/mol and is unlikely to be the overall rate-determining step in acetic acid hydrogenolysis. In the thermal evolution of acetic acid on Pd(111), the reaction-limited desorption of CO occurs at about 490 K (11). Experiments suggest that the formation of acetyl is the likely precursor to the formation of CO from C_2 oxygenates (13). Acetate and hydrogen recombine to form acetic acid, which can desorb at temperatures significantly lower than that at which surface acetyl species appear. This suggests that acetyl formation from acetate is likely to have a greater activation barrier than acetic acid formation and *may* be rate controlling for hydrogenolysis.

In their study of ethyl acetate hydrogenolysis over Cu/SiO_2, Agarwal *et al.* spectroscopically identified the acetyl intermediate under *in situ* hydrogenation conditions (2). This suggests that the acetyl species has significant surface lifetimes and is not rapidly hydrogenated to the acetaldehyde or the alcohol. If we assume that the same may hold true for Pd surfaces, this suggests that acetyl hydrogenation to acetaldehyde may also be a kinetically significant step.

Agarwal *et al.* studied the hydrogenation of acetaldehyde to ethanol and the hydrogenolysis of ethyl acetate to ethanol over Cu/SiO_2 under identical catalyst composition and reaction conditions (2, 3). They demonstrated that the turnover frequency (TOF) for acetaldehyde to ethanol is roughly 6000 times higher than that for ester hydrogenolysis, under otherwise identical reaction conditions (2, 3). Recently, Rachmady and Vannice also determined that the TOF for acetaldehyde hydrogenation on Pt/TiO_2 catalysts is 1000-fold higher than that for acetic acid hydrogenolysis (43). If we extend their observations to acetic acid hydrogenolysis over Pd, we might expect that the elementary steps in the hydrogenation of acetaldehyde to ethanol are unlikely to be overall rate controlling for acetic acid hydrogenolysis.

In summary, we speculate that the formation of acetyl from acetic acid, and its subsequent hydrogenation to acetaldehyde, are likely to be rate-controlling processes in the hydrogenolysis of acetic acid on Pd, by the mechanism shown in Fig. 4. The reaction coordinates for these two elementary steps are analyzed in greater detail in the following sections.

3.3. Pd(111) Catalyzed Hydrogenolysis of Acetic Acid to Acetaldehyde

In the proposed mechanism, the hydrogenolysis of acetic acid first involves the dissociation of acetic acid to form a surface acetyl species. The acetyl intermediate is subsequently hydrogenated to form acetaldehyde. It is likely that both of these steps are kinetically significant during carboxylic acid hydrogenolysis. We therefore examined in detail the reaction coordinate for both these steps. In Section 3.3.1, we analyze the dissociation of acetic acid to acetyl on Pd(111). In Section 3.3.2, we examine the second step, acetyl hydrogenation to acetaldehyde.

3.3.1. Dissociation of acetic acid to acetyl on Pd(111). In Section 3.1, we proposed that the dissociation of acetic acid to acetyl is the energetically favored pathway for hydrogenolysis. This was based on the analysis of the overall reaction energies. In Fig. 1A we showed two different paths by which this dissociation may occur. The first path involved the direct unimolecular dissociation of acetic acid via C–OH breaking thus resulting in the formation of acetyl($H_3C–C{=}O^*$) and hydroxyl (OH^*) surface species. This is identified as Rxn (5) in Fig. 1A and was computed to be +18 kJ/mol *endothermic*. The surface hydroxyl intermediate can subsequently be hydrogenated to water as shown in Rxn (8) of Fig. 1A. In the second path, both of these steps occur simultaneously. This hydrogen-assisted C–OH bond activation step [Rxn (6) in Fig. 1A] is calculated to be *exothermic* by 20 kJ/mol.

Figure 5 depicts the DFT results for the reactant, transition state, and product states along the reaction coordinate for the direct dissociation of acetic acid to acetyl and hydroxyl on Pd(111). DFT slab calculations were performed using a (2×3) unit cell, which corresponds to 0.17 monolayer (ML) coverage of acetic acid. At the initial state for hydrogenolysis, we propose that the acetic acid is bound in an η^1 geometry through the oxygen of the carbonyl group. This is an energetically stable adsorption state but is still 18 kJ/mol less favorable than the di-σ adsorption of acetic acid through the two oxygen atoms (see Scheme 1). The η^1 adsorption mode provides a more optimal starting structure for C–OH activation through the di-σ mode. At higher coverages, the η^1 mode may actually be more favored in that the steric repulsion interactions between species are less.

In the η^1 mode the C–OH bond of acetic acid is more easily activated over a surface Pd atom. The DFT-optimized transition state for this reaction is shown in Fig. 5b.

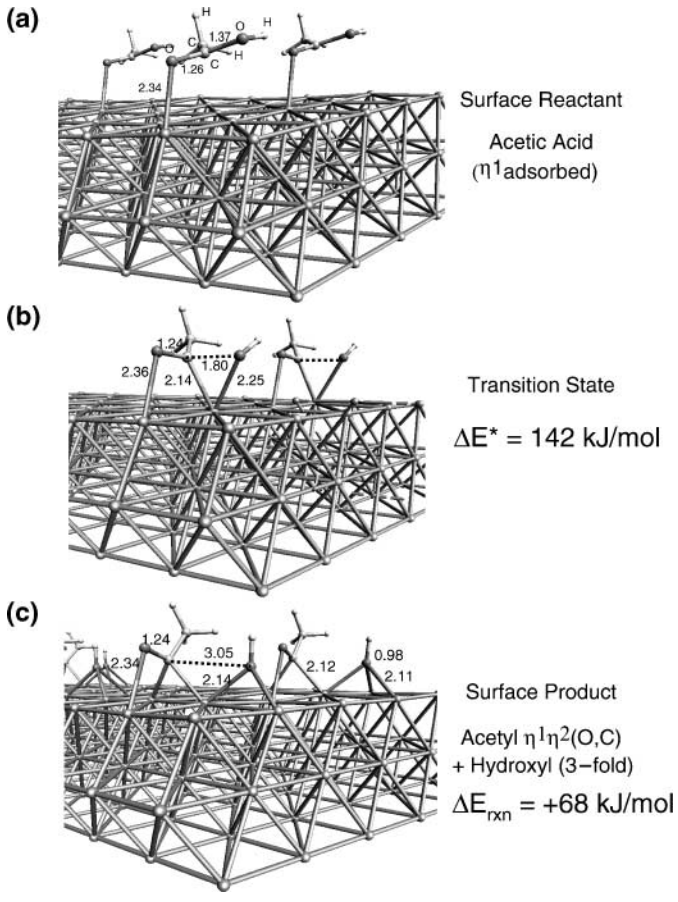

FIG. 5. DFT-computed reaction path for the dissociation of acetic acid to acetyl and hydroxyl intermediates on Pd(111). (a) η^1-bound acetic acid on Pd(111); (b) transition state for C–O bond activation of acetic acid; and (c) $\eta^1\eta^2$(O,C) bound acetyl and 3-fold hydroxyl species on Pd(111). Surface coverage of acetic acid = 0.17 monolayer.

The three-centered transition state shows a relatively long C–O bond (1.8 Å), which is 0.43 Å longer than the C–OH bond distance in acetic acid (1.37 Å). The Pd–O distance (2.25 Å) at the transition state geometry is 0.1 Å longer than at the final product state. The dissociated products are most favorably adsorbed in threefold hollow sites.

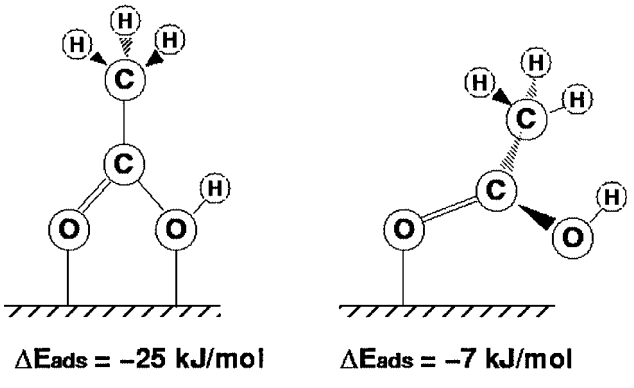

SCHEME 1

The acetyl species that forms is bound in the $\eta^1\eta^2$ mode, with the oxygen end on an atop site and the carbon end directed over a twofold bridge site (see Fig. 5c).

DFT calculations indicate that for 0.17 ML coverage of the Pd(111) surface, the activation barrier for C–OH bond breaking of acetic acid is +142 kJ/mol. The overall reaction energy is +68 kJ/mol endothermic. The reaction energy, in the absence of all lateral interactions, was calculated to be +18 kJ/mol. The reaction energy calculated here for the (2 × 3) unit cell is 50 kJ/mol more endothermic. This difference in the overall reaction energy is primarily due to the strong repulsive interactions at the product state (acetyl* + OH*) for the higher coverage (2 × 3) unit cell. The reaction is likely to be less endothermic for larger unit-cell dimensions, i.e., lower surface coverage. We have not explicitly examined coverage effects for this reaction in this paper.

It is possible that surface hydrogen may help to facilitate the dissociation process by reacting directly with the hydroxyl ligand. However, our initial attempts at isolating a transition state for this hydrogen-assisted path failed to identify a favorable path. For a surface hydrogen atom to assist the C–OH activation of acetic acid, it is necessary that it adsorb in close proximity to the acetic acid species. However, for such an adsorption geometry, we find that the repulsive interactions alone between hydrogen and acetic acid force the weakly bound acetic acid off the surface. It is possible that, on more reactive metals such as Re or Mo, the acetic acid is more strongly bound to the surface, thus allowing for a more stable hydrogen-assisted path for C–OH bond breaking. For the purposes of our discussion, we will assume that the C–OH bond breaking and H–OH coupling steps do not take place concertedly but occur instead in a sequential manner.

3.3.2. Coupling of acetyl and hydrogen to acetaldehyde on Pd(111). The acetyl intermediate that forms on Pd is subsequently hydrogenated to acetaldehyde. We carried out detailed studies of the reaction coordinate for this step to isolate a possible transition state. Figure 6 depicts the DFT-optimized reactant, transition state, and product structures along the reaction coordinate for the hydrogenation of acetyl to acetaldehyde over Pd(111) for a (2 × 3) unit cell (0.17 ML coverage). At the reactant state, both acetyl and hydrogen are adsorbed in threefold hollow sites. The reaction coordinate involves C–H bond formation over a surface Pd atom, along with the simultaneous migration of both acetyl and hydrogen toward one another during the coupling. In the transition state (see Fig. 6b), the C–H bond distance (1.75 Å) is still significantly longer than in the product acetaldehyde, where the C–H bond distance is about 1.1 Å. The three-centered transition state structure that results has a Pd–C distance of 2.24 Å, which is significantly longer than the Pd–C distance in the reactant acetyl (2.08 Å). The Pd–H distance at the transition state (1.54 Å) is characteristic of hydrogen bound to a low-coordination

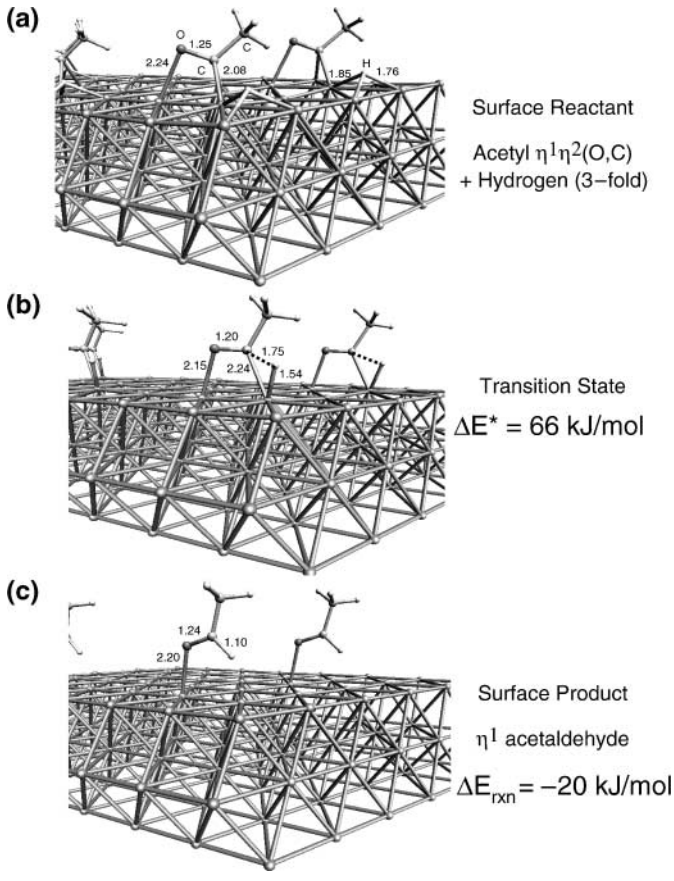

FIG. 6. DFT-computed reaction path for the hydrogenation of acetyl to acetaldehyde on Pd(111). (a) $\eta^1\eta^2$(O,C) bound acetyl and 3-fold hydrogen species on Pd(111); (b) transition state for C–H bond formation of acetyl; and (c) η^1-bound acetaldehyde on Pd(111). Surface coverage of acetaldehyde = 0.17 monolayer.

atop site on Pd(111). The transition state structure optimized for the hydrogenation of acetyl to acetaldehyde is very similar to transition states computed for other C–H bond activation reactions such as ethylene hydrogenation (35, 36).

DFT calculations indicate an activation barrier of +66 kJ/mol for the hydrogenation of adsorbed acetyl to acetaldehyde over Pd(111). The reaction is exothermic by 20 kJ/mol. Again, the differences in the calculated overall reaction energy reported here, versus those reported in Section 3.1, are due to strong lateral repulsive interactions at the higher 0.17 ML coverage. In this case the lateral interactions are more significant in the reactant (acetyl* + H*) state than in the product acetaldehyde state, thus making the reaction more exothermic than that calculated for the zero-coverage limit.

Based on our results, it appears that the dissociation of acetic acid to acetyl is likely the rate-controlling step in acetic acid hydrogenolysis over Pd(111). In the next section, we examine structure–property relationships for acetic acid hydrogenolysis over different Pd–Re surfaces.

3.4. Structure–Property Relationship for Acetic Acid Hydrogenolysis on Metal Surfaces

In an effort to develop simple structure–property relationships, we calculated the activation barriers for the two critical steps discussed in the previous section, the C–OH activation of acetic acid and acetyl hydrogenation over Pd(111), Re(0001), and Pd_{ML}/Re(0001) [pseudomorphic monolayer of Pd on Re(0001)] surfaces. In previous papers we have shown that the electronic interactions between Pd and Re in the Pd_{ML}/Re(0001) surface shift the average d-band position away from the Fermi energy to lower binding energies, as compared to both Pd(111) and Re(0001) (36, 38, 39). This electronic perturbation in Pd_{ML}/Re(0001) generally weakens the interaction of atomic and molecular adsorbates with the pseudomoprhic overlayer surface (36, 38, 39). The Re(0001) surface has more holes in the valence d band than Pd(111) and exhibits stronger adsorption energies than both Pd(111) and Pd_{ML}/Re(0001).

Table 3 shows the DFT-computed reaction energies and activation barriers for the dissociation of acetic acid to acetyl and hydroxyl on Pd–Re surfaces. Calculations suggest that the C–O bond activation of acetic acid is highly endothermic over Pd_{ML}/Re(0001) and Pd(111) surfaces with calculated reaction energies of +86 and +68 kJ/mol, respectively. The activation barriers for this reaction are quite high at +158 kJ/mol over Pd_{ML}/Re(0001) and +142 kJ/mol on Pd(111). On Re(0001), however, the barrier is significantly reduced ($\Delta E_{act} = +90$ kJ/mol). The overall reaction energy over Re is actually exothermic at −32 kJ/mol. These results are consistent with experimental observations that suggest that it is easier to activate the C–O bond on metal surfaces that readily form metal oxides (28). This suggests that C–O bond activation of acetic acid to form acetyl is energetically more favorable on Re(0001) than it is on Pd(111) and is least favorable on the Pd_{ML}/Re(0001) surface. Another important observation from Table 3 is that the microscopic reverse reaction for the coupling of acetyl and hydroxyl fragments occurs relatively easily on Pd_{ML}/Re(0001) and Pd(111), where the barrier is only about 70 kJ/mol. The

TABLE 3

DFT-Computed Activation Barriers and Reaction Energies for the Dissociation of Acetic Acid to Acetyl and OH Fragments for a (2 × 3) Unit Cell (Coverage = 0.17 ML Acetic Acid)[a]

Surface	ΔE_{rxn} C–OH bond breaking (kJ/mol)	$\Delta E_{activation}$(forward) C–OH bond breaking (kJ/mol)	$\Delta E_{activation}$(reverse) acetyl + OH coupling (kJ/mol)
Pd_{ML}/Re(0001)	+86	+158	+72
Pd(111)	+68	+142	+74
Re(0001)	−32	+90	+122

[a] $CH_3COOH^* + {}^* \rightarrow CH_3CO^* + OH^*$.

TABLE 4

DFT-Computed Activation Barriers and Reaction Energies for the Hydrogenation of Acetyl to Acetaldehyde for a (2 × 3) Unit Cell (Coverage = 0.17 ML Acetaldehyde)[a]

Surface	ΔE_{rxn} C–H bond formation (kJ/mol)	$\Delta E_{activation}$(forward) C–H bond formation (kJ/mol)	$\Delta E_{activation}$(reverse) acetaldehyde C–H bond breaking (kJ/mol)
Pd_{ML}/Re(0001)	−39	+69	+108
Pd(111)	−20	+66	+86
Re(0001)	+23	+88	+65

[a] $CH_3CO^* + H^* \rightarrow CH_3CHO^* + {}^*$.

same coupling reaction, however, has a much higher activation energy (+122 kJ/mol) on the Re(0001) surface. This is because both the hydroxyl and acetyl fragments are very strongly bound to the Re(0001) surface as compared to the Pd-based surfaces. It is, therefore, difficult to break these strong surface bonds.

The second elementary reaction of interest involves the hydrogenation of acetyl to acetaldehyde. We examined this step also over Pd(111), Re(0001), and Pd_{ML}/Re(0001) surfaces. The DFT-calculated activation barriers and overall reaction enegies for this reaction are reported in Table 4. DFT calculations indicate that the acetyl hydrogenation reaction has a relatively low activation barrier over Pd(111) and Pd_{ML}/Re(0001) (∼65–70 kJ/mol). The barrier for this step is somewhat higher over Re(0001) (+88 kJ/mol). On the other hand, the microscopic reverse reaction, i.e., C–H bond activation of η^1-bound acetaldehyde, has the lowest activation energy over Re(0001) (+65 kJ/mol) and the highest activation barrier on Pd_{ML}/Re(0001) (+108 kJ/mol). The differences in the activation barriers for the microscopic reverse reaction (C–H bond breaking) over the various surfaces examined here are greater (∼50 kJ/mol) than the differences in the forward hydrogenation barriers (∼20 kJ/mol). This is primarily because the transition state for C–H bond formation occurs relatively early along the reaction coordinate for hydrogenation and is structurally more reactant-like.

The trends for both C–H bond making and breaking activation barriers seen here appear to be very similar to the trends we demonstrated in an earlier publication for the hydrogenation of maleic anhydride and dehydrogenation of maleic anhydryl (37). Our previous studies for ethylene hydrogenation to ethyl and ethylene dehydrogenation to vinyl have also shown similar trends in the C–H bond activation energies over the different transition metal surfaces (36).

We summarize our results in Fig. 7, which is a plot of the activation barriers for C–OH bond breaking of acetic acid and acetyl hydrogenation to acetaldehyde, as a function of the metal d-band center. Hammer, Nørskov, and others have shown that the metal d-band center can be used to correlate the heats of adsorption as well as the activation energies for various elementary surface reactions such as C–H, CO, and NO bond activation (16, 17, 29, 36, 37). We therefore plot the activation barrier against the d-band center to see whether or not a similar correlation can be established here. The resulting graph (Fig. 7) indicates that C–OH bond breaking of acetic acid is more favorable on surfaces where the d-band center is closer to the Fermi energy. On the other hand, the hydrogenation of acetyl to acetaldehyde appears to be more favorable on surfaces where the d-band center is further away from the Fermi level. For transition metal elements having more than five d electrons, the d-band center shifts away from the Fermi energy as we move from left to right across the periodic table (45). Figure 7 indicates that, on metals to the left in the periodic table, C–OH bond breaking occurs more easily than it does over metals on the right. Hydrogenation, on the other hand, shows the opposite trend where metals on the left are less active than metals on the right. C–OH activation is likely the difficult step for metals to the right whereas hydrogenation is likely the difficult step for metals on the left. There appears to be a balance between these two steps that occur somewhere around Re. Rhenium is active for C–OH activation whereas Pd and Pd/Re are active for hydrogenation.

3.5. Effects of Alloying Pd/Re

A close analysis of the results presented in Fig. 7 indicates that this chemistry might be more optimally carried out over a bimetallic Pd/Re particle where Pd would be used for hydrogenation while Re would be used to carry out C–OH activation. Figure 8 schematically illustrates a simple design of a possible surface ensemble that can effectively carry out the hydrogenolysis of acetic acid to acetaldehyde via the mechanism proposed here. The active site here would

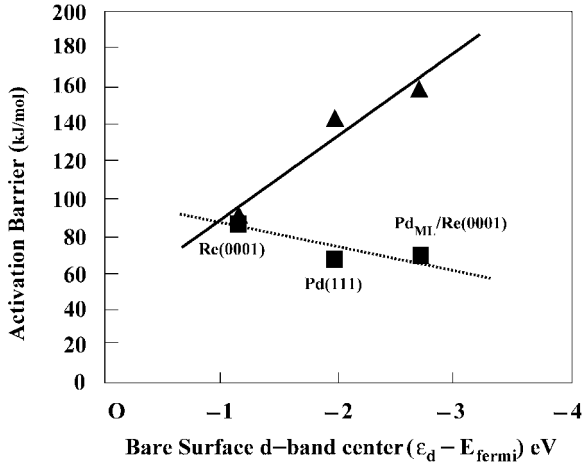

FIG. 7. Activation barrier for acetic acid C–OH bond breaking (▲) and acetyl hydrogenation (■) as a function of the bare metal surface d-band center. Calculated d-band centers are from Ref. 39.

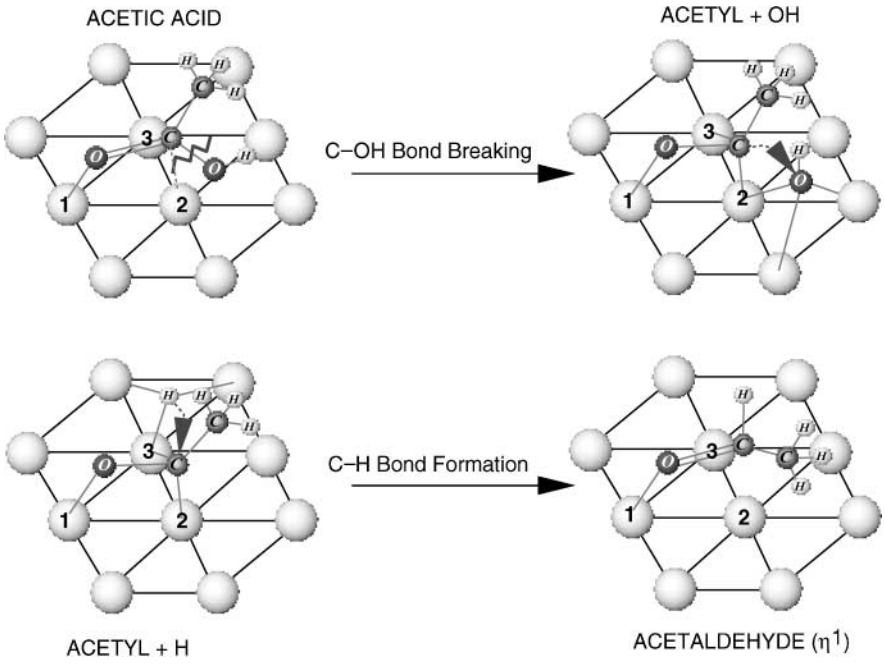

FIG. 8. Schematic illustration of surface ensemble likely to be involved in the hydrogenolysis of acetic acid to acetaldehyde over Pd(111).

involve five metal surface atoms, which include a threefold site and a neighboring bridge site. Acetic acid adsorbs at surface atom 1. The C–OH bond is activated at a neighboring surface metal atom site 2. The resulting fragments, i.e., acetyl and hydroxyl, bind at neighboring threefold hollow sites that share a single metal atom (metal atom 2). The acetyl fragment that is formed is then hydrogenated at the α-carbon position to form acetaldehyde. This hydrogenation step may occur over metal atom 2 or metal atom 3 on the surface.

Since metal atom 1 is principally involved in anchoring acetic acid on the surface and metal atom 2 is the metal atom that inserts into the C–OH bond, we would expect that substituting metal atoms 1 and 2 on a Pd(111) surface by Re atoms would facilitate C–OH bond breaking. We therefore reexamined the hydrogenolysis of acetic acid to acetaldehyde on Pd(111) by replacing metal atoms 1 and 2 which make up the threefold surface site with Re atoms. DFT calculations indicate that this $Pd_{0.33}Re_{0.66}$ surface alloy leads to an activation barrier of +113 kJ/mol for acetic acid C–OH bond breaking. The elementary reaction is mildly endothermic by +17 kJ/mol. The activation barrier of +113 kJ/mol is 29 kJ/mol lower than that for the pure Pd(111) surface (+142 kJ/mol) for the same reaction but is slightly higher than the activation barrier of 90 kJ/mol on Re(0001). This agrees well with our intuitive expectations.

The hydrogenation of acetyl to acetaldehyde was also examined on the alloyed Pd–Re overlayer. We examined the hydrogenation of acetyl over a Pd site (metal atom 3 in Fig. 8). The activation barrier was calculated to be +82 kJ/mol, whereas the overall energy of reaction was endothermic by 5 kJ/mol. Thus, it appears that alloying Re atoms into the Pd(111) surface facilitates C–OH bond activation relative to pure Pd(111). In addition, the alloy lowers the barrier for the hydrogenation of the acetyl intermediate from +88 kJ/mol over pure Re(0001) to +82 kJ/mol (over the $Pd_{0.33}Re_{0.66}$ alloy).

One should note that the results discussed herein assume that Re remains a zero-valent metal under the high hydrogen partial pressures. We cannot, however, exclude the fact that Re may also exist as an oxide.

3.6. Nonselective Paths in Acetic Acid Hydrogenolysis on Pd(111)

The principal decomposition products formed by acetic acid reactions on metal surfaces are CO, CO_2, and methane (11, 14). Barteau and co-workers have critically examined the surface reactions of C_2-oxygenates such as acetic acid, acetaldehyde, and ethanol on Pd-surfaces and postulated mechanisms for decomposition based on their TPD and EELS data (12–14, 49, 50). They suggest that the decomposition of surface-bound acetate to CO_2 is initiated by β C–H bond activation of the methyl group on acetate, following which the C–C bond is broken to release CO_2. The β C–H bond activation of acetate is speculated to be rate determining in the decomposition of acetate to form CO_2. In the presence of hydrogen, the resulting methylene fragment that forms is hydrogenated to methane. Shekhar and Barteau propose that the decomposition of C_2-oxygenates, such as acetic acid and acetaldehyde, to CO is preceded by the formation of surface-bound acetyl intermediate (50).

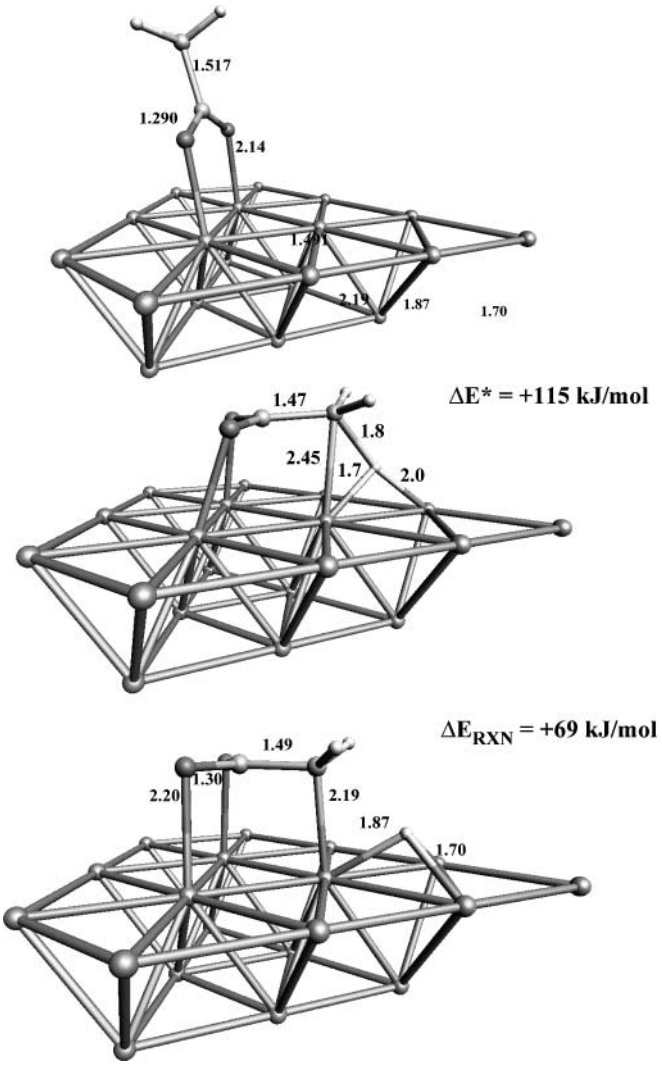

FIG. 9. DFT-computed transition state geometry for the β C–H bond activation of acetate on Pd(111). β C–H bond activation of acetate is believed to be the rate-determining step in the decomposition of acetate to CO_2 on Pd(111).

The acetyl species undergoes C–C bond scission to liberate CO and methyl surface fragments.

In a previous paper, we used DFT to examine in detail the reaction coordinate for β C–H bond activation of acetate on Pd(111) (34). Figure 9 shows the DFT-computed transition state geometry for β C–H bond breaking of acetate. Calculations indicate that the reaction has a high activation barrier (+115 kJ/mol) and is endothermic by +69 kJ/mol on Pd(111) (34). This is slightly higher than the experimentally measured overall activation barrier of +85 kJ/mol for acetate decomposition, estimated from the UHV-TPR data of Davis and Barteau (11, 14). Based on our studies of C–H bond activation reactions (34–37), we find that C–H bond-breaking reactions are generally more favored on reactive surfaces such as Re, which form strong metal adsorbate bonds. This is because C–H bond breaking is primarily guided by electron back-donation into the antibonding σ^*_{CH} orbital. The d bands for metals such as Re are energetically more favorably situated to back-donate to this adsorbate's antibonding orbital. The dissociation products are also more strongly bound to metals such as Re, than to Pd(111). We therefore expect acetic acid dissociation to CO and CO_2 to be more favored on metals such as Re, compared to Pd(111). This is consistent with UHV experimental observations that indicate greater amounts of CO and CO_2 being formed on surfaces such as Rh(111) than on Pd(111) during the thermal evolution of acetic acid on these surfaces (14, 19, 21). The surface science results indicate that acetate reacts to form CO_2 and CO with little evidence for the formation of other intermediates that subsequently decompose to form CO and CO_2. We therefore restricted our study to acetate and acid acid. Under working conditions, ethanol and acetaldehyde may also go on to form CO.

The catalysis of carboxylic hydrogenolysis involves a delicate balance between C–O bond-breaking activity and β C–H bond-breaking activity. Metals such as Re, which easily activate the C–O bond of acetic acid, are also good at the β C–H bond scission of acetate. Therefore, the overall reaction selectivity to ethanol is poor. Metals such as Pd, on the other hand, may provide better selectivity but cannot easily activate the C–O bond. A bimetallic surface composed of reactive metals, such as Re, and Group VIII metals, such as Pd, may provide the optimal balance between C–O bond activation and hydrogenation activity, resulting in a good overall catalytic performance for acid hydrogenolysis.

4. SUMMARY AND CONCLUSIONS

A detailed series of first-principles quantum chemical calculations were carried out over Pd(111) to quantify the binding energies and determine the reaction energies for an array of plausible steps. These results indicate that the most favorable path for acetic acid hydrogenolysis involves the formation of an acetyl intermediate, followed by its hydrogenation to acetaldehyde. Acetaldehyde is then subsequently hydrogenated to form ethanol. Acetyl formation and acetyl hydrogenation to acetaldehyde appear to be kinetically significant steps. Detailed reaction coordinate calculations were therefore used to isolate the transition states for these elementary reactions. DFT results indicate that C–OH bond activation of acetic acid on Pd(111) is highly endothermic (+68 kJ/mol) and has a fairly high activation barrier (+142 kJ/mol). Acetyl hydrogenation on Pd(111), on the other hand, is exothermic by 20 kJ/mol and has a much lower activation barrier (+66 kJ/mol). C–O bond activation is therefore likely to be the rate determining on the Pd-based surfaces.

The results indicate that there is an inverse correlation between the activation barriers for C–OH activation and

hydrogenation over the three different metal surfaces examined. The barriers for C–OH bond activation observe the following trend:

$$\mathrm{Re(0001)\ [90\ kJ/mol]} < \mathrm{Pd(111)\ [142\ kJ/mol]} < \mathrm{Pd_{ML}/Re(0001)\ [158\ kJ/mol]}.$$

The barriers for acetyl hydrogenation, in contrast, follow nearly the exact opposite trend:

$$\mathrm{Pd(111)\ [66\ kJ/mol]} < \mathrm{Pd_{ML}/Re(0001)\ [69\ kJ/mol]} < \mathrm{Re(0001)\ [88\ kJ/mol]}.$$

DFT calculations suggest that C–OH activation is more favored on metals to the left in the periodic table such as Re(0001) than on metals to the right. The overall reaction energies for the products that form are stabilized on Re due to the stronger binding energies for the intermediates on Re. This ultimately leads to a more exothermic reaction (for C–OH activation) over metals to the left than metals to the right. Re(0001) therefore provides a nominal activation barrier for acetic acid C–OH bond activation. Rhenium alone, however, is not optimal since it also leads to acetic acid decomposition routes. However, Group VIII metals such as Pd demonstrate lower activation barriers for hydrogenation and reduced acetic acid decomposition (i.e., they exhibit better selectivity), but they tend to display poor activity for acetic C–O bond dissociation (hydrogenolysis). The reduction in acetic acid decomposition is consistent with experimental observations (14, 19, 21).

Optimum carboxylic acid hydrogenolysis, therefore, appears to involve an intricate balance between C–O activation and C–H bond formation steps, and C–H bond scission. Catalysts that are capable of preferentially activating the C–O bond, without significantly enhancing β C–H bond activation of the carboxylic acid, are likely to be good catalysts for acid hydrogenolysis. The ensemble size requirements for acid decomposition and acid hydrogenolysis are different. A bimetallic Pd–Re catalyst, with suitably atomically dispersed Re ensembles on Pd, may provide the optimal trade-off between hydrogenolysis and decomposition activity, rendering it an effective catalyst for acid hydrogenolysis.

ACKNOWLEDGMENTS

We are grateful to the DuPont Chemical Company and the National Science Foundation (CTS-9702762) for their partial support of this work. We also thank the National Computational Science Alliance for a portion of the computational resources necessary to carry out this work. We are also grateful to Professor Jurgen Hafner and Dr. Georg Kresse of the Universitaet Wien for the use of their code VASP.

REFERENCES

1. Aas, N., and Bowker, M., *J. Chem. Soc. Faraday Trans*. **89**, 1249 (1993).
2. Agarwal, A. K., Cant, N. W., Wainwright, M. S., and Trimm, D. L., *J. Mol. Catal*. **43**, 79 (1987).
3. Agarwal, A. K., Wainwright, M. S., Trimm, D. L., and Cant, N. W., *J. Mol. Catal*. **45**, 247 (1988).
4. Andzelm, J., *in* "Density Functional Methods in Chemistry" (J. Labanowski and J. Andzelm, Eds.), p. 155. Springer-Verlag, New York, 1991.
5. Andzelm, J., and Wimmer, E., *J. Chem. Phys*. **96**, 1280 (1992).
6. Becke, A., *ACS Symp. Ser*. **394**, 165 (1989).
7. Becke, A. D., *Phys. Rev. A* **38**, 3098 (1988).
8. Bowker, M., and Madix, R. J., *Appl. Surf. Sci*. **8**, 299 (1981).
9. Cavani, F., *Chim. Industria* **77**, 791 (1996).
10. Claus, P., Lucas, M., and Lucke, B., *Appl. Catal. A: Gen*. **79**, 1 (1991).
11. Davis, J. L., and Barteau, M. A., *Langmuir* **5**, 1299 (1989).
12. Davis, J. L., and Barteau, M. A., *J. Am. Chem. Soc*. **111**, 1782 (1989).
13. Davis, J. L., and Barteau, M. A., *Surf. Sci*. **235**, 235 (1990).
14. Davis, J. L., and Barteau, M. A., *Surf. Sci*. **256**, 50 (1991).
15. Evans, J. W., Wainwright, M. S., Cant, N. W., and Trimm, D. L., *J. Catal*. **88**, 203 (1984).
16. Hammer, B., Morikawa, Y., and Nørskov, J. K., *Phys. Rev. Lett*. **76**, 2141 (1996).
17. Hammer, B., and Nørskov, J. K., *Surf. Sci*. **343**, 211 (1995).
18. Harris, N., and Tuck, M. W., *Hydrocarbon Process*. **69**, 79 (1990).
19. Hoogers, G., Papageorgepoulos, D. C., Ge, Q., and King, D. A., *Surf. Sci*. **340**, 23 (1995).
20. Houtman, C. J., and Barteau, M. A., *J. Catal*. **130**, 528 (1991).
21. Houtman, C. J., Brown, N. F., and Barteau, M. A., *J. Catal*. **145**, 37 (1994).
22. Kitson, M., and Williams, P. S., The British Petroleum Company, London, U.S. Patent 4,985,572, 1991.
23. Kittel, C., "Introduction to Solid State Physics," 6th ed., Wiley, New York, 1986.
24. Kohler, M. A., Cant, N. W., Wainwright, M. S., and Trimm, D. L., *Proc. Int. Congr. Catal*. **9**, 1043 (1988).
25. Kresse, G., and Furthmuller, J., *Comput. Mat. Sci*. **6**, 15 (1996).
26. Mabry, M., Prichard, W., and Ziemecki, S., E. I. DuPont de Nemours and Company, U.S. Patent 4,550,185, 1985.
27. Mabry, M., Prichard, W., and Ziemecki, S., E. I. DuPont de Nemours and Company, U.S. Patent 4,609,636, 1986.
28. Masel, R. I., "Principles of Adsorption and Reaction on Solid Surfaces." Wiley, New York, 1996.
29. Mavrikakis, M., Hammer, B., and Nørskov, J. K., *Phys. Rev. Lett*. **81**, 2819 (1998).
30. Miya, B., Kao Soap Company, Ltd., Japan, U.S. Patent 3,894,054, 1975.
31. Miya, B., Hoshino, F., and Matuda, M., Kao Soap Company, Ltd., Japan, U.S. Patent 3,580,930, 1971.
32. Natal Santiago, M. A., Sanchez-Castillo, M. A., Cortright, R. D., and Dumesic, J. A., *J. Catal*. **193**, 16 (2000).
33. Neurock, M., *in* "Dynamics of Surfaces and Reaction Kinetics in Heterogeneous Catalysis" (G. F. Froment and K. C. Waugh, Eds.), Studies in Surface Science and Catalysis, Vol. 109, Elsevier Science, Amsterdam, 1997.
34. Neurock, M., *Appl. Catal. A: Gen*. **160**, 169 (1997).
35. Neurock, M., and Pallassana, V., *in* "Transition State Modeling for Catalysis" (D. K. Truhlar and K. Morokuma, Eds.), Symp. Series Vol. 721, Chap. 18. American Chemical Society, Washington DC, 1999.
36. Pallassana, V., and Neurock, M., *J. Catal*. **191**, 301 (2000).
37. Pallassana, V., and Neurock, M., *J. Phys. Chem. B* **104**, 9449 (2000).
38. Pallassana, V., Neurock, M., and Coulston, G. W., *J. Phys. Chem. B* **103**, 8973 (1999).
39. Pallassana, V., Neurock, M., Hansen, L. B., Hammer, B., and Nørskov, J. K., *Phys. Rev. B* **60**, 6146 (1999).
40. Payne, M. C., Teter, M. P., Allan, D. C., Arias, T. A., and Joannopoulos, J. D., *Rev. Mod. Phys*. **64**, 1045 (1992).

41. Perdew, J. P., *Phys. Rev. B* **33**, 8822 (1986).
42. Perdew, J. P., Chevery, J. A., Vosko, S. H., Jackson, K. A., Pederson, M. R., Singh, D. J., and Fiolhais, C., *Phys. Rev. B* **46**, 6671 (1992).
43. Rachmady, W., and Vannice, M. A., *J. Catal.* **192**, 322 (2000).
44. "Butanediol, Product Focus Report," Source: BASF, Chemical Week, 1998.
45. Ruban, A., Hammer, B., Stoltze, P., Skriver, H. L., and Nørskov, J. K., *J. Mol. Catal. A: Chem.* **115**, 421 (1997).
46. Schoofs, G. R., and Benziger, J. B., *Surf. Sci.* **143**, 359 (1984).
47. Schwartz, J. T., E. I. DuPont de Nemours and Company, U.S. Patent 5,478,952, 1995.
48. Sharif, M., and Turner, K., Davy McKee Ltd., England, 1986.
49. Shekhar, R., and Barteau, M. A., *Catal. Lett.* **31**, 221 (1995).
50. Shekhar, R., Barteau, M. A., Plank, R. V., and Vohs, J. M., *J. Phys. Chem. B* **101**, 7939 (1997).
51. Sim, W. S., Gardner, P., and King, D. A., *J. Am. Chem. Soc.* **118**, 9953 (1996).
52. Stuve, E. M., Jorgensen, S. W., and Madix, R. J., *Surf. Sci.* **146**, 179 (1984).
53. Turek, T., Trimm, D. L., and Cant, N. W., *Catal. Rev.—Sci. Eng.* **36**, 645 (1994).
54. Vosko, S. J., Wilk, L., and Nusair, M., *Can. J. Phys.* **58**, 1200 (1980).
55. Westerwelt, R., *Chem. Week* 9 (1999).
56. Wood, A., *Chem. Week* 19 (1995).
57. Yan, T. Y., Albright, L. F., and Case, L. C., *Ind. Eng. Chem. Prod. Res. Dev.* **4**, 101 (1965).
58. Ziegler, T., *Chem. Rev.* **91**, 651 (1991).